INORGANIC CHEMISTRY FRONTIERS

CCS 中国化学会 CHINESE CHEMICAL SOCIETY

ROYAL SOCIETY OF CHEMISTRY

RESEARCH ARTICLE

View Article Online
View Journal | View Issue

Cite this: *Inorg. Chem. Front.*, 2020, **7**, 689

The effect of the electronic structure and flexibility of the counteranions on magnetization relaxation in $[Dy(L)_2(H_2O)_5]^{3+}$ (L = phosphine oxide derivative) pentagonal bipyramidal SIMs†

Ismael F. Díaz-Ortega, [a] Juan Manuel Herrera, *[a] Sourav Dey, [b] Hiroyuki Nojiri, *[c] Gopalan Rajaraman *[b] and Enrique Colacio *[a]

Received 30th October 2019,
Accepted 1st December 2019

DOI: 10.1039/c9qi01412h

rsc.li/frontiers-inorganic

We report here a new Dy^{III}-SIM $[Dy(OPCy_3)_2(H_2O)_5](CF_3SO_3)_3{\cdot}2OPCy_3$ ($OPCy_3$ = tricyclohexylphosphine oxide) with a pentagonal bipyramidal geometry, which exhibits a blocking temperature T_B = 8.5 K and an anisotropy barrier U_{eff} = 562 K. *Ab initio* calculations show that this complex exhibits the largest U_{calc} = 732 K among the Dy^{III}-SIM complexes containing the $[Dy(L)_2(H_2O)_5]^{3+}$ (L = phosphine oxide derivative) cationic unit, which is essentially due to the electronic effects of the triflate anion that increase the charge difference between the oxygen atoms of the ligands L coordinated in axial positions and those belonging to the equatorial water molecules. This charge difference enhancement, which is also reflected in a larger difference between the corresponding Dy–O distances (Δ), appears to be the driving force to increase the U_{calc} value. The comparatively smaller experimental U_{eff} value observed for this compound has been justified by the flexibility of the structural network due to the size of the triflate counteranions. The absence of a clear correlation between T_B and U_{eff} (or U_{calc}) suggests the involvement of Raman and QTM mechanisms in the magnetization relaxation process.

Introduction

The field of molecular magnetism based on coordination compounds has experienced enormous development since the discovery of Single-Molecule Magnets (SMMs) during the nineties.[1] These unique nanomaterials are discrete metal complexes, in which the molecular magnetization is blocked either parallel or antiparallel to the magnetic field when the polarizing field is removed below T_B (blocking temperature). As a result, SMMs exhibit slow relaxation of the magnetization and magnetic hysteresis at the molecular level. In addition to these classical features of SMMs, they can show quantum properties, such as quantum tunnelling of magnetization (QTM), quantum phase interference and quantum coherence.[1] SMMs are interesting not only due to these fascinating physical properties but also due to their foreseeable applications in quantum computing, data storage and spintronics.[2] The ultimate target in this field is the incorporation of SMMs in functional devices.

The magnetization blockade arises from the existence of an energy barrier for the magnetization reversal (U_{eff}) along the bistable magnetic ground state. The magnitude of U_{eff}, which is related to the energy gap between the ground and first (or higher) excited states, essentially depends on the magnetic anisotropy.[1,3] In this context, lanthanide ions have gained increasing relevance for constructing SMMs due to their inherent strong single-ion magnetic anisotropy and large unquenched orbital angular momentum.[4] Among lanthanide containing SMMs, those mononuclear in nature (also named single-ion magnets, SIMs) are at the forefront of the research in the field, because their magnetic anisotropy can be deliberately controlled by an appropriate choice of the lanthanide ions and ligands.[4d–h] Thus, the electronic and steric features of the ligands (electron density and distribution of the donor atoms and steric size of the ligands and substituents) determine the coordination geometry and the ligand field around

[a]*Departamento de Química Inorgánica, Facultad de Ciencias, Universidad de Granada, Avda. Fuentenueva s/n, 18071 Granada, Spain. E-mail: ecolacio@ugr.es*
[b]*Department of Chemistry, Indian Institute of Technology Bombay, Powai, Mumbai 400076, India*
[c]*Institute for Materials Research, Tohoku University, Katahira, Sendai, 980-8577, Japan*

†Electronic supplementary information (ESI) available. CCDC 1957205. For ESI and crystallographic data in CIF or other electronic format see DOI: 10.1039/c9qi01412h

the lanthanide ion and, therefore, the ground state magnetic anisotropy in SIMs.[4] In this regard, experimental and *ab initio* theoretical calculations have shown that, in the case of Dy^{3+} complexes, a strong axial crystal field is mandatory to observe SIM behaviour.[5] The axial field leads to an axial anisotropy where the doublet ground state has the largest m_J values (±15/2). This Kramers doublet will be more stabilized as the electrostatic repulsion of its oblate electron density with the axial ligands is larger than that with the equatorial ligands as much as possible.[6] In fact, experimental results for high efficiency bis(cyclopentadienyl)Dy^{III}-SIMs has shown that the presence of equatorial coordinated isocarbonyl ligands has a detrimental effect on the T_B of the $[Dy(Cp)]^+$ counterparts.[7] Nevertheless, tiny transverse components of the anisotropy, as well as weak dipolar and hyperfine interactions, could allow the fast Quantum Tunneling of the Magnetization (QTM) between the two components of the doublet ground state that takes a shortcut through the energy barrier, thus making the remnant magnetization at zero field dissappear.[1] In fact, most of the Dy^{3+}-based SMMs show rapid decay of hysteresis loops at zero-field with no remnant magnetization.[8] In some cases, magnetic dilution with the Y^{3+} counterpart allows observation of remnant magnetization at zero-field, due to the strong suppression of intermolecular dipolar interactions enabling active QTM.[9] In some compounds, despite the larger U_{eff} values after magnetic dilution (>1000 K), the remnant magnetization occurs at surprisingly very low temperature.[9] In order to justify this observation, it has been postulated that flexible lattices are responsible for fast relaxation, so that the vibrational characteristics of a specific SMM play an important role in the relaxation dynamics.[10] It should be noted at this point that the presence of a high-order symmetry axis favours the collinearity of the anisotropic axes of the excited and ground states and, therefore, the relaxation through higher excited states.[11] This ultimately leads to higher U_{eff} values.

In view of the above considerations, a good strategy to access SMMs with high U_{eff} and T_B parameters would be that of preparing Dy^{3+} complexes with (i) high-order symmetry axes, (ii) high electron density axial ligands and neutral poor electron density equatorial ligands (or without equatorial ligands) and (iii) rigid networks to avoid rapid relaxation. The experimental results confirm the significance of this strategy as several Dy^{3+} complexes with trigonal bipyramidal,[12] square antiprismatic,[13] sandwich[7,14] and pentagonal bipyramidal[15] geometries have been shown to exhibit SMM behaviour at zero field with U_{eff} and T_B values as large as 2217 K (ref. 7*c*) and 80 K,[7c] respectively. Among these SIM (single-ion magnet) Dy^{3+} complexes, those exhibiting a pentagonal–bipyramidal geometry (PBPY-7) occupy a relevant place[15] showing values of U_{eff} and T_B as high as 1815 K (ref. 15*b*) and around 30 K,[15d] respectively. For these Dy^{3+} SIMs an experimental magneto-structural correlation has been established, which indicated that the U_{eff} values depend linearly on the axial Dy–X bond lengths.[15i]

Moreover, recently *ab initio* studies on this kind of compound indicated that the removal of not only the equatorial ligands, but also the outer-sphere molecules and anions enhances the barrier for magnetization reversal.[15d,g]

This result prompted us to prepare a new PBPY-7 Dy^{3+} complex $[Dy(OPCy_3)_2(H_2O)_5](CF_3SO_3)_3{\cdot}2OPCy_3$ (**1**) belonging to the family of SIM complexes of the general formula $[Dy(L)_2(H_2O)_5]X_3{\cdot}L_n$ (L = $OPCy_3$, X = Cl, Br, n = 1, 2;[15a] $OP^tBu(NH^iPr)_2$, X = I, n = 2 [15d] HMPA X = Cl, I, n = 1, 2 [15g] and $OpCyPh_2$, X = Br, N = 2 [15f] Cy = cyclohexyl, HPMA = hexamethylfosforamide), which contains triflate counteranions instead of halide anions. The main aim of this work is to compare the SIM properties of **1** with those exhibited by its analogous complexes and to draw some conclusions about the effects of the electronic structure, size and flexibility of outer-sphere molecules and anions on the SIM properties.

Results and discussion

Compound **1** was obtained by the reaction of dysprosium triflate, $Dy(CF_3SO_3)_3$, with Cy_3PO using a **1 : 2** molar ratio methanol/water (1/4) mixture. Air stable single-crystals suitable for X-ray crystallography appeared after slow evaporation of the solution at room temperature. The structure of **1** (Fig. 1) consists of $[Dy(OPCy_3)_2(H_2O)_5]^{3+}$ cationic units, three triflate anions and two free $OPCy_3$ ligands. The latter two ($OPCy_3$ and triflate anions) are connected to the cationic unit by hydrogen bonds.

Within the cationic unit, as observed in the analogous complexes containing halide counteranions,[15a,b,d,f,g] the Dy^{3+} ion exhibits a pentagonal bipyramidal (PBPY-7) geometry, where two $OPCy_3$ ligands occupy the axial positions, whereas the five coordinated water molecules are located in the equatorial plane defining an almost regular pentagon. The Dy–O axial bond distances are shorter than the equatorial ones (average values of 2.202 Å and 2.362 Å, respectively), so that the cationic units exhibit a compressed PBPY-7 geometry with a O–Dy–O

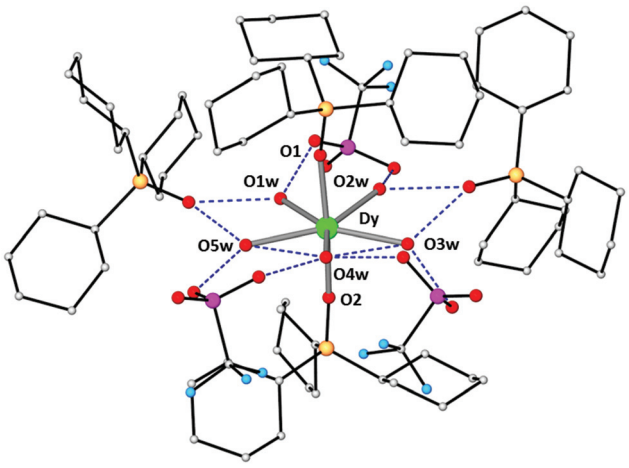

Fig. 1 Perspective view of the structure of complex **1**. Code colours: dysprosium (green), oxygen (red), fluorine (blue), sulphur (orange), and carbon (grey).

Table 1 Magneto-structural data for complexes containing the psudo-D_{5h} $[Dy(L)_2(H_2O)_5]^{3+}$ unit

$[Dy(L)_2(H_2O)_5]^{3+}$ SIMs	U_{cal} (K)	U_{eff} (K)	$T_{B(ZFC)}$ (K)	Shortest Dy···Dy (Å)	CShMs (D_{5h})	Ref.
$[Dy(OPCy_3)(H_2O)_5](triflate)_3{\cdot}2OPCy_3$ (**1**)	732	562	8.5	12.642	0.639	T.w.
$[Dy(OPCy_3)(H_2O)_5]Br_3{\cdot}2OPCy_3{\cdot}2H_2O{\cdot}2EtOH$ (**1a**)	573	543	11	11.230	0.239	15*a*
$[Dy(OPCy_3)(H_2O)_5]Cl_3{\cdot}OPCy_3{\cdot}H_2O{\cdot}EtOH$ (**1a′**)	645	472	8	8.420	0.142	15*a*
$[Dy(OP^tBu(NH^iPr)_2(H_2O)_5]I_3{\cdot}2OP^tBu(NH^iPr)_2{\cdot}(H_2O)$ (**1b**)	688	651	12	10.819	0.224	15*d*
$[Dy(HMPA)_2(H_2O)_5]I_3{\cdot}2HMPA$ (**1c**)	640	600	7	11.767	0.131	15*g*
$[Dy(HMPA)_2(H_2O)_5]Cl_3{\cdot}HMPA$ (**1c′**)	584	460	7	9.026	0.154 0.284	15*g*
$[Dy(OPCyPh_2)(H_2O)_5]Br_3{\cdot}2OPCy_3{\cdot}3H_2O{\cdot}EtOH$ (**1d**)	427	466	10.5	13.826	0.174	15*f*

angle along the axial axis of 173.48° and Ow–Dy–Ow angles in the equatorial plane between 71.64 and 74.03° (average value of 72.38°). These structural parameters point out that the DyO_7 polyhedron is very close to an ideal D_{5h} polyhedron (180° and 72°), which is supported by the low value of the continuous shape measure (CShM)[16] parameter for an ideal D_{5h} of 0.64 (see Table 1 and Table S1†). The coordinated water molecules in the equatorial plane are involved in hydrogen bond interactions with two of the oxygen atoms of each triflate anion and the oxygen atom of each free $OPCy_3$ ligand. The former form six short hydrogen bonds with O···O donor–acceptor distances in the range 2.720–2.806 Å (average value of 2.756 Å), whereas the latter are involved in four hydrogen bonds with O···O donor–acceptor distances in the range 2.613–2.672 Å (average value of 2.631 Å). The most significant differences between **1** and the analogous compound previously reported by Tang and col. also containing two free $OPCy_3$ ligands and bromide counteranions of formula $[Dy(OPCy_3)(H_2O)_5]Br_3{\cdot}2OPCy_3{\cdot}2H_2O{\cdot}2EtOH$ (**1a**) are: (i) the water molecules and the oxygen and sulphur atoms in the outer coordination sphere form a 16-membered ring in **1** and a 10-membered ring in **1a**. (ii) Each triflate forms two out-of-plane hydrogen bonds, which leads to deviations of the water molecules from the equatorial plane in the 0.037–0.226 Å range (average value of 0.16 Å), whereas in **1a** the water molecules are almost in the plane with deviations in the 0.0–0.15 Å range (average value of 0.05 Å). (iii) The O···X donor–acceptor distances involving water molecules and counteranions are shorter in **1** than in **1a** (in this case O···Br distances are around 3.2 Å). (iv) the O–Dy–O angle in the pseudo-axial C_5 axis is smaller by around 6° in **1** than in **1a**. (v) The shortest Dy···Dy intermolecular distance of 12.642 Å is longer than that observed in compound **1a** (11.23 Å). It should be noted that recently three complexes of formulae $[Dy(OP^tBu(NH^iPr)_2(H_2O)_5]I_3{\cdot}2OP^tBu(NH^iPr)_2{\cdot}(H_2O)$[15*d*] (**1b**), $[Dy(HMPA)_2(H_2O)_5]I_3{\cdot}2HMPA$[15*g*] (**1c**) and $[Dy(OPCyPh_2)(H_2O)_5]Br_3{\cdot}2OPCyPh_2{\cdot}3H_2O{\cdot}EtOH$ (**1d**)[15*f*] have been reported, which are structurally very similar to **1** and **1a** but have $OP^tBu(NH^iPr)_2$, hexamethylphosphoramide and $OPCyPh_2$, respectively, as axial ligands and iodide and bromide as counteranions. The only significant difference between these compounds and **1a** is that in **1b–1d** the three iodide anions in the outer coordination sphere occupy consecutive positions, whereas in **1a**, as in **1**, only two bromide anions are in neighboring positions, and separated from the third anion by the non-coordinated molecules of the respective phosphine–oxide ligand. Therefore, it seems that triflate counteranions are responsible for the structural differences indicated above in issues i–v. Because of these differences the structure of **1** is not so close to the ideal D_{5h} symmetry as the structures of **1a–1c** (see continuous shape measures in Table 1).

Magnetic properties

The static dc magnetic properties of **1** were measured on a powder polycrystalline sample in the 2–300 K temperature range under an applied magnetic field of 0.1 T. The temperature dependence of $\chi_M T$ (χ_M is the molar magnetic susceptibility) is shown in Fig. 2.

At 300 K, the $\chi_M T$ value of 14.00 cm^3 K mol^{-1} is very close to that expected for an isolated Dy^{3+} ion ($4f^9$, J = 15/2, S = 5/2, L = 5, g = 4/3, $^6H_{15/2}$) in the free ion approximation (14.18 cm^3 K mol^{-1}). On cooling, the $\chi_M T$ product steadily decreases to 10 K to reach a value of 12.7 cm^3 K mol^{-1}. This slight decrease is due to the thermal depopulation of excited $\pm m_j$ sublevels, which arise from the splitting of the spin–orbit ground term $^6H_{15/2}$ by the crystal field effects, and points out the existence of a large magnetic anisotropy with well separated low-lying energy levels. Below 10 K, the $\chi_M T$ product sharply decreases to reach a value of 6.03 cm^3 K mol^{-1} at 2 K, which is typical of

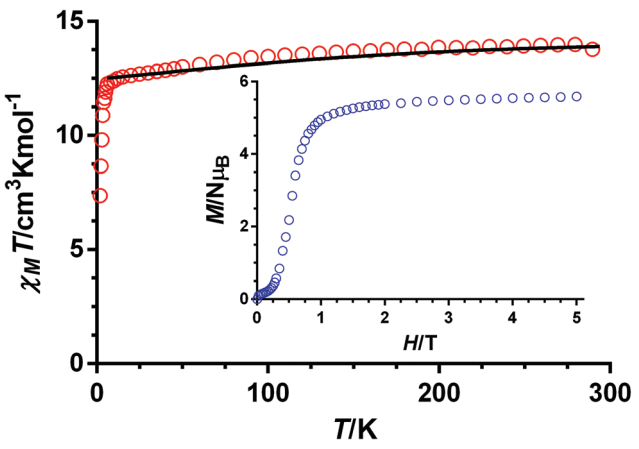

Fig. 2 Temperature dependence of $\chi_M T$ for compound **1**. The solid line corresponds to the *ab initio* CASSF computed temperature dependence of the $\chi_M T$ product at 0.1 T for **1**. Field dependence of the magnetization for **1** (inset).

high efficiency Dy-SMMs and is due to the onset of magnetic blocking. As expected for this kind of SMM, the field dependence of the magnetization at 2 K (Fig. 2, inset) shows a sinusoidal behavior at a low field with a saturation value of $5.58N\mu_\beta$ at 5 T. This low saturation value confirms the axial nature (±15/2) of the well-isolated ground state. The temperature dependence of the field cooled (FC) and zero-field cooled (ZFC) magnetization data for **1** (Fig. 3, left) diverge at 8.5 K with the maximum in the ZFC magnetization at the same temperature, which corresponds to the magnetic blocking temperature, T_B. The diluted complex **1@Y** (Dy/Y ~ 1/9) exhibits a similar behaviour with the maximum at 8 K (Fig. S1†). It is worth noting that this compound shows small butterfly shaped hysteresis loops at 2 K using a magnetic field sweep rate of 1.8 mT s^{-1} (Fig. S2†), without visible remnant magnetization and coercitive field at zero field. In view of this and to confirm the blocking of magnetization in this compound, we have also measured the magnetization curve in a full cycle pulsed magnetic field at 0.4 K and 1.6 K (Fig. 3 right and Fig. S3†). The maximum field applied ranges from 1.7 to 18.7 T, and the sweep rate depends on the maximum-pulsed field and is higher for 18.7 T. In addition, it is worth mentioning that the magnetic field strength is not symmetric for the magnet between the positive and the negative directions during the pulsing (Fig. S4†). Magnetization curves at 0.4 K and at 1.6 K show hysteresis loops with a coercitive field of ~4.5 T at the maximum sweep rate with clear remnant magnetization and slow reversal of magnetization around zero field. No saturation is observed at low fields until we reach 5–7 T (due to the high U_{eff} of **1**) and we need around 20 T to observe full saturation of the system. Finally, as expected for SMMs, the hysteresis increases with the increase of the sweeping rate. The relaxation around zero field indicates a sharp reversal of ~40% of the magnetization value due to adiabatic magnetization reversal most probably caused by unsuppressed QTM.

Alternating current (ac) magnetic susceptibility measurements in the 1–1400 Hz frequency range under zero external magnetic field and with an oscillating field of 3.5 Hz were carried out to study the slow relaxation of the magnetization. The in-phase (χ'_M) and out-of-phase (χ''_M) components of the ac susceptibility show frequency dependent peaks (Fig. 4 and Fig. S5†) with well-defined maxima in the χ''_M *vs.* *T* plot (Fig. 4)

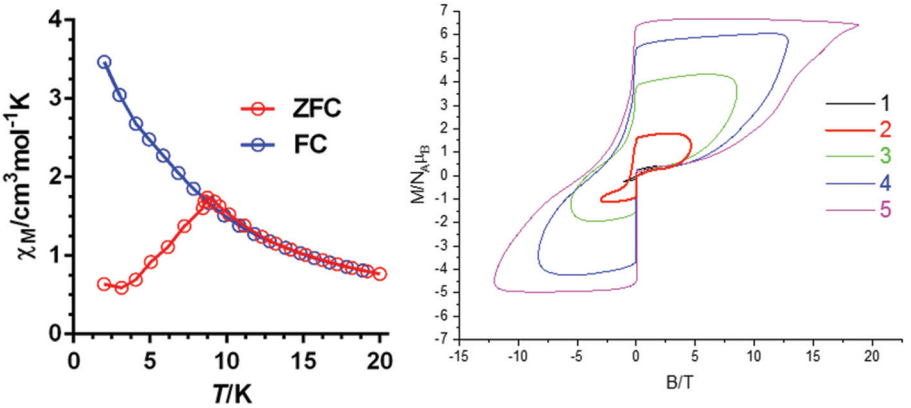

Fig. 3 Temperature dependence of zero-field cooled (red) and field cooled (blue) magnetization for **1** (a). Pulsed-field magnetization curves for **1** at maximum applied fields of 1.7, 4.6, 8.4, 12.7 and 18.7 T (1–5).

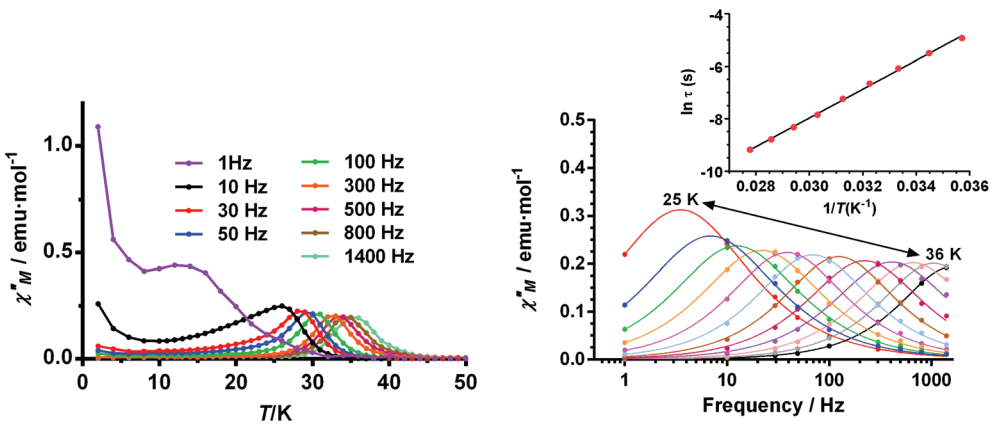

Fig. 4 Temperature and frequency dependence of the out-of-phase component of the ac susceptibility (χ''_M) for compound **1**. Temperature dependence of the relaxation times in the form of the Arrhenius plot (inset).

in the temperature range 12.0 K (1 Hz)–36.0 K (1400 Hz), which points out a high energy barrier for magnetization reversal. The relaxation times were extracted from the frequency dependence of χ''_M at different temperatures using the generalized Debye model. The extracted relaxation times for the high temperature region (28 K–36 K, where only the Orbach process occurs) were fitted with the Arrhenius equation affording an effective energy barrier U_{eff} = 562 (7) K and a pre-exponential factor $\tau_0 = 1.7(5) \times 10^{-11}$ s. Below 28 K, Raman and QTM processes would be operative (corresponding to a broadening of the peaks in the low frequency range; see Fig. 4, right).

The fitting of χ''_M *vs.* χ'_M (Cole–Cole plot, Fig. S6†) for **1** shows a narrow distribution of relaxation times in the high temperature region with values of α in the range 0.11 (28 K)–0.007 (36 K), which indicate the existence of almost a unique relaxation process.

Ac measurements on the diluted complex **1@Y** (Dy/Y = 1/9) show that the relative intensity of the tail at very low temperature due to QTM is slightly reduced with respect to the pristine compound **1**. However, this presumably weak reduction of the QTM does not have any noticeable effect on the Orbach process, as the peaks of the χ''_M signals for each frequency appear at the same temperature as for **1** and the U_{eff} and τ_0 values of 552 (51) K and 1.4 (30) $\times 10^{-11}$ s, respectively, are rather similar to those extracted for **1** (see Fig. S7 and S8†). This fact is not unexpected as the QTM and Orbach processes occur at temperature regions far apart from each other.

In order to gain further insights into the mechanism of relaxation of compound **1** and how the change of the counteranions, as well as the number, type and distribution of phosphine–oxide ligands, affect the magnetization relaxation and the value of the thermal energy barrier, we performed *ab initio* CASSCF/RASSI-SO/SINGLE-ANISO calculations using the MOLCAS 8.2 software (see the ESI†). All the calculations were carried out on the crystal structure of **1**. This methodology has been proved very useful in rationalizing and predicting the electronic structure and relaxation mechanism of SIM complexes.[17] The computed eight KDs belonging to $^6H_{15/2}$ span up to 778.1 cm^{-1}. The temperature dependence of $\chi_M T$ calculated from the spectrum of computed energy levels for **1** (Tables S2–S4†) reproduce rather well the experimental temperature dependence of $\chi_M T$ (Fig. 2). The ground KD is a pure $m_J = |\pm 15/2\rangle$ state with $g_{xx} = g_{yy} < 1.10^{-4}$ and g_{zz} = 19.97; the anisotropy g_{zz} axis lies closely along the pseudo-C_5 axis (the deviation between the g_{zz} axis and O–Dy–O axial direction is 5.9°; see Fig. S9†). The negligible transverse anisotropy in the ground KD suggests the absence of QTM at this state. The first excited state (KD1), which lies 341.7 cm^{-1} above the ground KD, is almost a pure m_J $|\pm 13/2\rangle$ state with g_{xx} = 0.17, g_{yy} = 0.024 and g_{zz} = 17.086. As KD1 is strongly axial, quenching of the QTM is also expected at this level. The g_{zz} is almost parallel to the anisotropy axis of the ground state (deviation of 3.7°) and therefore it is not probable that the magnetization relaxation occurs through KD1. However, the second excited Kramers doublet (KD2) (a mixture of m_J $|\pm 1/2\rangle$, m_J $|\pm 3/2\rangle$ and m_J $|\pm 11/2\rangle$), which lies at 508.5 cm^{-1} above the ground state, has important transverse components of the *g*-tensor (g_{xx} = 0.766 g_{yy} = 1.774 and g_{zz} = 17.815) and the g_{zz} anisotropy axis deviates 84.5° from the orientation of the ground state g_{zz} axis. In view of these facts, it is reasonable to assume that the relaxation in **1** is more likely to occur through KD2 and then the calculated energy barrier is U_{cal} = 727.8 K, which is rather higher than the experimental U_{eff} value of 562 K. This fact could be due, among other factors, to dipolar intermolecular interactions and the flexibility of the structural network, which are not taken into consideration in the type of *ab initio* calculation used and favor the shortcut of the thermal energy barrier for magnetization reversal.[10] The computed values of the transverse magnetic moments connecting the three first KDs together to their corresponding energy values are given in Fig. 5. The values of transverse magnetic moments help us further understand the relaxation mechanism operating in **1**.

The ground and first excited states show very small, almost negligible, transverse magnetic moment values of 0.75 $\times$ $10^{-4}\mu_B$ and 0.69 $\times$ $10^{-2}\mu_B$, respectively, thus indicating that QTM and TA-QTM are almost suppressed for these KDs. Moreover, the transverse moment for the Orbach process connecting the ground and first excited states of opposite magnetization is very small (0.4 $\times$ $10^{-3}\mu_B$) and therefore this relaxation pathway is not operative. However, the TA-QTM relaxation process through the second excited state is predominant with a transverse magnetic moment of 1.58μ_B. The above considerations based on the values of the transverse magnetic moments confirm the above-indicated statement derived from the transverse anisotropy that the magnetic relaxation in **1** takes place through the second excited state.

It is worth noting that among the SIM complexes with pseudo-D_{5h} symmetry containing two phosphine oxide derivatives in axial positions and five water molecules in the equatorial plane (see Table 1 and Table S5†), where all U_{cal} values were calculated at the same level of approximation for comparative purposes, compound **1** shows the higher U_{cal}.

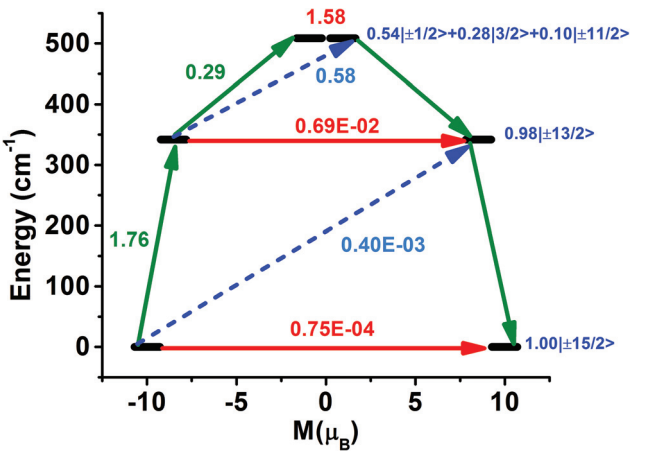

Fig. 5 Possible relaxation pathways in **1**. The black lines indicate the KDs as a function of the magnetic moments. Red lines denote QTM in the ground state and TA/QTM through the first and second excited states. Blue dashed lines represent possible Orbach processes.

At first glance, this result could be considered as unexpected, because some of the structural features of this complex, such as the smaller O–Dy–O angle and the larger deviations of the water molecules from the equatorial plane, indicate that the structure of **1** is not so close to the ideal D_{5h} as the structures of the other SIMs shown in Table S5† (compound **1** has by far the largest CShM value for PBPY-7). In this rationale, we have assumed for these closely related complexes that when the structure gets closer to ideal D_{5h}, the axial crystal field becomes stronger and, consequently, the SIM properties would improve. However, it is clear from the theoretical calculation results that, even though these structural factors exert some effect on the properties of SIMs, they are not the essential issues in determining the properties of SIMs in this type of pseudo-D_{5h} complex with large O–Dy–O angles and small deviations of the water molecules from the equatorial plane (see Table S5†). In view of this, we have performed a LoProp charge analysis (see the ESI†) of **1** and the analogous complexes containing the ligand $OPCy_3$ and Cl^- and Br^- as counteranions, $[Dy(OPCy_3)(H_2O)_5]Br_3{\cdot}2OPCy_3{\cdot}2H_2O{\cdot}2EtOH$ (**1a**) and $[Dy(OPCy_3)(H_2O)_5]Cl_3{\cdot}OPCy_3{\cdot}H_2O{\cdot}EtOH$ (**1′a**), respectively (Fig. S10, S11 and S12†). The results derived from this study (Tables S6–S8†) show that: (i) the LoProp charges on the oxygen atoms of the $OPCy_3$ ligands, which are coordinated in axial positions of the pseudo-D_{5h} DyO_7 coordination sphere, are slightly larger for compound **1** (average value: 1.128*e*) than for complexes **1a** and **1′a** (average values of ~1.115*e*) and (ii) the calculated charges for the oxygen atoms of the water molecules coordinated in the equatorial pentagonal plane are smaller for **1** (0.74*e*) than for **1a** and **1′a** (~0.76*e*). As the difference between the axial and equatorial electrostatic repulsions (related to the difference in Loprop charges) is larger for compound **1** than for **1a** and **1′a**, the former has a stronger axial ligand field with smaller transverse anisotropy than complexes **1a** and **1′a**, which explains why **1** exhibits the higher value of U_{cal}. In view of this, the main factor controlling the U_{cal} in this type of pseudo-D_{5h} complex appears to be the difference between axial and equatorial charges in the inner coordination sphere, so that the larger this difference, the stronger the axial field and then the U_{calc} value. It is worth mentioning that the shortest Dy–O distances involve the oxygen atoms with the largest charges, and then there should also exist a correlation between Δ (difference between the Dy–Ow distances in equatorial positions and the $Dy–O_{P–O}$ distances in axial positions of the PBPY-7 coordination environment) and U_{calc}. In fact, for $[Dy(L)_2(H_2O)_5]^{3+}$ SIMs, U_{calc} increases as Δ increases. Specifically, for SIM complexes of general formula $[Dy(L)_2(H_2O)_5]X_3{\cdot}2L$ (**1** and **1a–1d**) there exists a linear correlation between U_{calc} and Δ (see Fig. 6).

Additionally, the comparative analysis of the above LoProp charge results for **1**, **1a** and **1′a** clearly indicates that the outer coordination sphere plays an important role in determining the transverse anisotropy and then the U_{cal}. In this regard, complexes **1a** and **1**, which show very similar structural parameters in the inner coordination sphere, however, present important changes in the outer coordination sphere, where

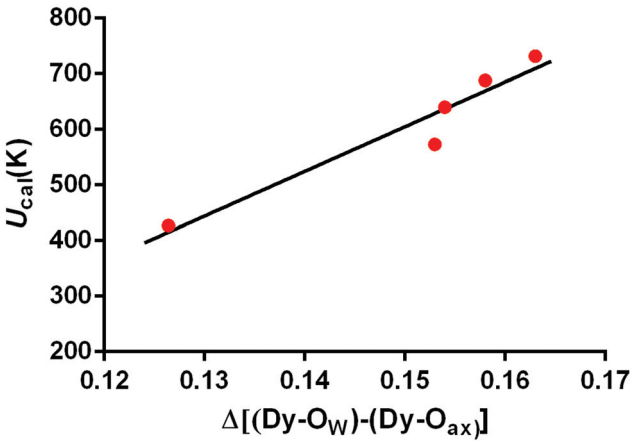

Fig. 6 Correlation between U_{calc} and Δ for $[Dy(L)_2(H_2O)_5]X_3{\cdot}2L$ complexes (**1** and **1a–1d**).

the Br^- anions in **1a** are replaced by triflate in **1**. In this latter compound, both the spreading of the negative charge of the triflate anions and the electron-withdrawing effect of the trifluoromethyl group lead to a reduction of the charge on the oxygen atoms. This charge reduction results in a weaker transverse ligand field and a higher U_{cal} value. In order to evaluate the effect of the elimination step-by-step of the anions/molecules in the inner and outer coordination spheres of **1** on the LoProp charges and U_{cal} values, we have calculated three additional model compounds built from the crystal structure of **1** (**1A**, **1B**, and **1C**). Model **1A** corresponds to the elimination of two $OPCy_3$ molecules in the outer coordination sphere, **1B** is obtained by the additional elimination of the three triflate anions and **1C** corresponds to the $[Dy(OPCy_3)]^{3+}$ species (see Fig. S13†). On passing from **1A** to **1C**, the average values of LoProp charges (Tables S9–S11†) on the oxygen atoms in apical positions increase from 1.14*e* to 1.17*e* and to 1.21*e*, whereas the charges on the oxygen atoms in equatorial positions simultaneously decrease from 0.71*e* to 0.68*e* and zero, respectively. Therefore, the consecutive removal of the ligands $OPCy_3$, triflate anions and finally water molecules causes an increase in the strength of the axial ligand field, which ultimately results in an increase of the U_{cal} values from 924 K (**1A**) to 1136 K (**1B**) and to 3093 K (**1C**) (Tables S12–S14†). It is worth mentioning that the two latter values are virtually identical to those previously reported for the analogous models derived from the complex $[Dy(HMPA)_2(H_2O)_5]I_3{\cdot}2HMPA$ (**1c**). The fact that the U_{calc} value for model **1A** is about 200 K higher than those obtained for the analogous model complexes derived from **1c** highlights again the superior effect of the triflate anions compared to I^- anions for creating a stronger axial ligand field. Likewise, this result reflects the important role of the features of the counteranion (size and charge distribution) in determining the value of the energy barrier for magnetization reversal.

The experimental values of U_{eff} extracted from the Arrhenius equation for the complexes $[Dy(L)_2(H_2O)_5]X_3{\cdot}L_n$

(see Table 1) generally follow the same order as the U_{calc} values, but there exist two anomalies: (i) U_{eff} values for complexes **1**, **1a′** and **1c′** are significantly lower than the U_{calc} values, and (ii) complex **1** exhibits a larger U_{calc} value than complexes **1b** and **1c**; however, the experimental U_{eff} values for the latter are larger than that for the former complex. In principle, one could think that both anomalies could be due to the dipolar intermolecular interactions, which were not accounted for by theoretical calculations. Dipolar interactions favour QTM and reduce the thermal energy barrier to an effective value.[1] This hypothesis could explain issue (i) for **1a′** and **1c′**, because the shortest Dy⋯Dy distances for compounds **1a′** and **1c′**, on which the dipolar interactions depend inversely, are rather smaller than those found for the rest of the compounds shown in Table 1. Bearing this in mind, it is expected that **1a′** and **1c′** exhibit larger QTM and therefore smaller U_{eff} values than the rest of the $[Dy(L)_2(H_2O)_5]X_3{\cdot}L_n$ compounds. Nevertheless, this suggestion should be taken with caution because, even though $[Dy(L)_2(H_2O)_5]X_3{\cdot}L_n$ complexes with Dy⋯Dy > ∼11 Å show no significant differences after dilution with diamagnetic Y^{III}, the results for those with Dy⋯Dy < ∼10 Å are contradictory. Thus for complexes **1b** [15d] and **1c** [15g] the dilution results in a significant increase in U_{eff}, whereas the U_{eff} for **1a** does not appear to significantly change after magnetic dilution.[15a] Moreover, the effect of the dipolar interactions can be discarded in the case of **1** as it exhibits the longest Dy⋯Dy distance. The Dy⋯Dy dipolar interactions can also be ruled out to explain issue (ii) because the Dy⋯Dy distance is longer for **1** than for **1b** and **1c**. In light of this, an alternative explanation for the observed phenomenon could be based on the flexibility of the lattice. In this regard, it has been recently suggested from experimental and theoretical results that the temperature dependence of the spin relaxation depends not only on the electronic structure but also on the vibrational characteristics of a particular SMM.[10] This is because the internal vibrations play an essential role in connecting the spin states and phonons that contribute to the spin-relaxation pathways. As flexible SMMs have more degrees of freedom that can combine with the local vibrations, it has been proposed that the magnetization relaxation can be accelerated in structurally flexible SMMs. In complexes **1b** and **1c**, each iodide counteranion is involved in two bifurcated hydrogen bonds with the coordinated water molecules, and the oxygen atoms of the water molecules and the phosphine oxide oxygen in the secondary coordination sphere form a 10-membered ring. However, in compound **1** two oxygen atoms of each triflate anion are involved in hydrogen bonds with the coordinated water molecules and these latter and the oxygen and sulphur atoms in the outer coordination sphere form a 16-membered ring. Moreover, the triflate anion has a bigger size and, obviously, is more flexible than the halide anions. These structural features could lead to a larger flexibility of the lattice of **1** and therefore to a more rapid relaxation in this compound.

Finally, it is worth mentioning that there is no clear correlation between the blocking temperature (T_B) determined from the maximum of the ZFC plot and either U_{eff} or U_{calc} (Table 1). This fact has been previously pointed out for SIMs with U_{eff} > 600 K.[18] For these compounds a linear correlation was established between $\log(T_B)$ and $\log \tau_{switch}$ (the temperature at which Raman relaxation takes over from the Orbach process), which demonstrated the crucial role of the Raman relaxation process in determining T_B. The dependence of T_B on τ_{switch} rather than on U_{eff} or U_{calc} could be, among other factors, also responsible for the absence of correlation between T_B and U_{eff} or U_{calc} in the complexes of the type $[Dy(L)_2(H_2O)_5]X_3{\cdot}L_n$.

Concluding remarks

The ongoing results demonstrate that the new air stable complex $[Dy(OPCy_3)_2(H_2O)_5]$ $(CF_3SO_3)_3{\cdot}2OPCy_3$ presents the largest *ab initio* calculated anisotropy barrier (U_{calc}) among the reported complexes containing the $[Dy(L)_2(H_2O)_5]^{3+}$ cationic unit (L = phosphine oxide derivative), where the DyO_7 coordination sphere exhibits a PBPY-7 geometry. LoProp charge calculations on complexes containing the $OPCy_3$ ligand indicate that the main factor controlling the U_{cal} in this type of pseudo-D_{5h} complex appears to be the difference between axial and equatorial charges in the inner coordination sphere, so that the larger this difference, the stronger the axial field and then the U_{calc} value. The electronic features of the triflate anion (spreading of the negative charge on the oxygen and sulphur atoms and the electron-withdrawing effect of the trifluoromethyl group) lead to a reduction of the charge on the oxygen atoms belonging to the coordinate water molecules, resulting in a weaker transverse ligand field and a higher U_{cal}. Given that the Dy–O distances become shorter as the charge on the oxygen atoms increases, there also exists a correlation between Δ (difference between the Dy–Ow distances in equatorial positions and the $Dy–O_{P–O}$ distances in axial positions of the PBPY-7 coordination environment) and U_{calc}, so that, for $[Dy(L)_2(H_2O)_5]^{3+}$ SIMs, U_{calc} increases as Δ increases. Interestingly for SIM complexes of general formula $[Dy(L)_2(H_2O)_5]X_3{\cdot}2L$ there appears to exist a linear correlation between U_{calc} and Δ. In this type of complex, the elimination of the non-coordinated ligands increases the U_{calc} value. This increase is rather higher for the complex with triflate counteranions than for complexes with halide counteranions. Although the experimental values of U_{eff} extracted from the Arrhenius equation for the complexes $[Dy(L)_2(H_2O)_5]X_3{\cdot}L_n$ are smaller than the U_{calc} values, they generally follow the same order as the latter. Nevertheless, the U_{eff} values for the compounds containing chloride counteranions are significantly smaller than the U_{calc} values, which could be tentatively due, among other reasons, to the relatively larger Dy⋯Dy dipolar interactions expected for these compounds (they present the shortest Dy⋯Dy distances) that favour QTM. The flexibility of the structure of $[Dy(OPCy_3)_2(H_2O)_5]$ $(CF_3SO_3)_3{\cdot}2OPCy_3$, essentially promoted by the larger size of the triflate anion with regard to the halide anions, could be at the origin of the smaller U_{eff} value observed for this compound compared to its analogues $[Dy(OP^tBu(NH^iPr)_2(H_2O)_5]I_3{\cdot}2OP^tBu(NH^iPr)_2{\cdot}(H_2O)$

and $[Dy(HMPA)_2(H_2O)_5]I_3{\cdot}2HMPA$. Finally, for complexes of the type $[Dy(L)_2(H_2O)_5]X_3{\cdot}L_n$ there is no clear correlation between T_B and U_{eff} or U_{calc}, which could suggest that the Raman relaxation process and QTM play a crucial role in determining T_B. In order to support the above hypotheses, we are preparing new $[Dy(L)_2(H_2O)_5]X_3{\cdot}L_n$ complexes where by altering the electronic structure and size of L and counteranions, Δ could be finely tuned and then U_{eff} and T_B.

Experimental

General procedures

Tricyclohexyl phosphine oxide (Cy_3PO), solvents and the corresponding lanthanide salt were purchased from commercial sources and used as received.

Preparation of complexes

$[Dy(H_2O)_5(Cy_3PO)_2]{\cdot}(CF_3SO_3)_3{\cdot}(Cy_3PO)_2$ (**1**): a solution of anhydrous $Dy(CF_3SO_3)_3$ (0.05 mmol) in a mixture of water : methanol (1 : 4, 5 mL) was added dropwise to a solution of Cy_3PO (0.10 mmol) in 5 mL of methanol. The resultant solution was kept at room temperature until complete evaporation of the solvent. Colourless crystals appropriate for X-ray crystallography were obtained in good yield (70–74%). Anal. calc. for 1 $C_{75}H_{142}S_3DyP_4O_{18}F_9$: C, 47.77; H, 7.59. Found: C, 48.12; H, 7.71. The diluted complex **1@Y** was prepared following the same method but using $Dy(CF_3SO_3)_3$ (0.005 mmol) and $Y(CF_3SO_3)_3$ (0.045 mmol). The Dy/Y ratio was determined to be 11.3% by SEM. The X-ray powder spectra of **1** and **1@Y** and that derived from the X-ray crystal structure show the purity of these isostructural complexes (Fig. S14†).

X-ray crystallography

Suitable crystals of complex **1** were mounted on a Bruker D8 Venture (Mo Kα radiation, λ = 0.71073 Å, Photon 100 CMOS detector). Details of the crystal, data collection and refinement parameters are given in the ESI (Table S15†). Once the data were processed (raw data integration, merging of equivalent reflections and empirical correction of the absorption), the structures were solved by direct methods and refined using full-matrix least-squares on weighted F^2 values using the SHELX suite of programs[19] integrated in Olex2.[20] Selected bond lengths and angles can also be found in the ESI (Tables S16 and S17†). A set of atoms F7T-F9T and O7T-O9T belonging to a triflate counterion are disordered over two sites and refined with site occupancies of 0.59/0.41. Carbon atoms C8–C12 that form one of the cyclohexyl rings in a cyclohexyl phosphine moiety are also disordered over two sites and refined with occupancies of 0.37/0.63. These disordered atoms are not shown in Fig. 1 for the sake of clarity. CCDC 1957205† contains the supplementary crystallographic data for this article.

Physical measurements

Elemental analyses were carried out at the "Centro de Instrumentación Científica" of the University of Granada on a Fisons-Carlo Erba analyser model EA 1108. Direct (dc) and alternating (ac) current susceptibility measurements were performed with a Quantum Design SQUID MPMS XL-5 device. Ac experiments were performed using an oscillating ac field of 3.5 Oe and frequencies ranging from 1 to 1400 Hz. Low-temperature magnetization measurements were performed using a conventional inductive probe in pulsed-magnetic fields. The temperature as low as 0.4 K was reached using a ^{3}He cryostat.[21] Polycrystalline specimens were mounted in a capillary tube made of polyimide. Samples of approximately 20 mg were not fixed within the sample tube and then they aligned along the magnetic field direction. Subsequently, a magnetic field was applied several times until the orientation effect was saturated and the magnetization curves obtained in further shots were found to be identical. SEM measurements were performed using a Hitachi S-510 Scanning Electron Microscope equipped with a Röntec M series EDX detector. Powder X-ray diffraction measurements of a polycrystalline sample of complex **1** were carried out in the 5–30° 2θ range on a Bruker D2 Phaser.

Computational methodology

Post–Hartree–Fock *ab initio* calculations were carried out on the crystal structure of **1** using the CASSCF + RASSI-SO + SINGLE_ANISO approach as implemented in the MOLCAS 8.2 suite.[22] Specially designed SINGLE_ANISO[23] enables calculations of anisotropic magnetic properties and g tensors for lowest Kramers doublets (KD). We have used [Dy.ANO-RCC...7s6p4d2f1g.], [S.ANO-RCC...4s3p.], [P.ANO-RCC...4s3p.], [F.ANO-RCC...3s2p.], [O.ANO-RCC...3s2p.], [C.ANO-RCC...3s2p.] and [H.ANO-RCC...2s.] contracted basis sets for dysprosium, sulphur, phosphorus, fluorine, oxygen, carbon and hydrogen atoms respectively.[24] In order to save disk space, Cholesky decomposition possessing a threshold of 0.2×10^{-7} was incorporated into our calculations.[25] The relativistic effect of the lanthanide ion has been taken into account by DKH Hamiltonian. An active space of the CASSCF[26] method was constructed considering nine electrons in seven 4f orbitals. Within this active space, we have computed 21 sextets states. Furthermore, the CASSCF computed spin-free states were mixed *via* the de RASSI module[27] to obtain the spin–orbit states. Atomic charges were calculated with the LoProp program[28] implemented in MOLCAS 8.2.

Conflicts of interest

There are no conflicts to declare.

Acknowledgements

Financial support from Ministerio de Economía y Competitividad (MINECO) for Projects CTQ2014-56312-P and PGC2018-102052-B-C21, the Junta de Andalucía (FQM-195), FEDER project A-FQM-172-UGR18 and the University of Granada is gratefully acknowledged. A part of this work was

carried out at HFLSM, IMR, Tohoku University. I. F. D. O. also acknowledges support by COLABS. GR would like to thank the SERB (CRG/2018/000430) for financial support. S. D. thanks the UGC for a Senior Research Fellowship.

References

1 (*a*) D. Gatteschi and R. Sessoli, Quantum tunneling of Magnetization and Related Phenomena in Molecular Materials, *Angew. Chem., Int. Ed.*, 2003, **42**, 268; (*b*) *Molecular Nanomagnets*, ed. D. Gatteschi, R. Sessoli and J. Villain, Oxford University Press, Oxford, 2006; (*c*) *Molecular Magnets: Physics and Applications*, ed. J. Bartolomé, F. Luis and J. F. Fernández, Springer-Verlag, Berlin-Heidelberg, 2014; (*d*) S. Gao, *Structure and Bonding*, Springer-Verlag, Berlin-Heidelberg, 2015, vol. 164; (*e*) J. J. Baldovi, S. Cardona-Serra, J. M. Clemente-Juan, E. Coronado, A. Gaita-Ariño and A. Palii, Rational Design of Single-Ion Magnets and Spin Qubits Based on Mononuclear Lanthanoid Complexes, *Inorg. Chem.*, 2012, **51**, 12565; (*f*) S. T. Liddle and J. van Slageren, Improving f-element single molecule magnets, *Chem. Soc. Rev.*, 2015, **44**, 6655.

2 (*a*) M. N. Leuenberger and D. Loss, Quantum computing in molecular magnets, *Nature*, 2001, **410**, 789; (*b*) A. R. Rocha, V. M. García-Suárez, S. W. Bailey, C. J. Lambert, J. Ferrer and S. Sanvito, Towards molecular spintronics, *Nat. Mater.*, 2005, **4**, 335; (*c*) A. Ardavan, O. Rival, J. L. Morton, S. J. Blundell, A. M. Tyryshkin, G. A. Timco and R. E. P. Winpenny, Will Spin-Relaxation Times in Molecular Magnets Permit Quantum Information Processing?, *Phys. Rev. Lett.*, 2007, **98**, 057201; (*d*) L. Bogani and W. Wernsdorfer, Molecular spintronics using single-molecule magnets, *Nat. Mater.*, 2008, **7**, 179; (*e*) M. Mannini, F. Pineider, P. Sainctavit, C. Danieli, E. Otero, C. Sciancalepore, A. M. Talarico, M.-A. Arrio, A. Cornia, D. Gatteschi and R. Sessoli, Magnetic memory of a single-molecule quantum magnet wired to a gold surface, *Nat. Mater.*, 2009, **8**, 194; (*f*) E. Coronado and A. Epstein, *J. Mater. Chem.*, 2009, **12**, 1661; (*g*) M. J. Martínez-Pérez, S. Cardona-Serra, C. Schlegel, F. Moro, P. J. Alonso, H. Prima-García, J. M. Clemente-Juan, M. Evangelisti, A. Gaita-Ariño, J. Sesé, J. Van Slageren, E. Coronado and F. Luis, Gd-Based Single-Ion Magnets with Tunable Magnetic Anisotropy: Molecular Design of Spin Qubits, *Phys. Rev. Lett.*, 2012, **108**, 247213; (*h*) G. Aromí, D. Aguilà, P. Gamez, F. Luis and O. Roubeau, Design of magnetic coordination complexes for quantum computing, *Chem. Soc. Rev.*, 2012, **41**, 537; (*i*) R. Vincent, S. Klyatskaya, M. Ruben, W. Wernsdorfer and F. Balestro, Electronic read-out of a single nuclear spin using a molecular spin transistor, *Nature*, 2012, **488**, 357; (*j*) M. Ganzhorn, S. Klyatskaya, M. Ruben and W. Wernsdorfer, Strong spin–phonon coupling between a single-molecule magnet and a carbon nanotube nanoelectromechanical system, *Nat. Nanotechnol.*, 2013, **8**, 165; (*k*) M. Jenkins, T. Hümmer, M. J. Marínez-Pérez, J. García-Ripoll, D. Zueco and F. Luis, Coupling single-molecule magnets to quantum circuits, *New J. Phys.*, 2013, **15**, 095007; (*l*) E. Coronado and M. Yamashita, Molecular spintronics: the role of coordination chemistry, *Dalton Trans.*, 2016, **45**, 16553; (*m*) M. Atzori, S. Benci, E. Morra, L. Tesi, M. Chiesa, R. Torre, L. Sorace and R. Sessoli, Structural Effects on the Spin Dynamics of Potential Molecular Qubits, *Inorg. Chem.*, 2018, **57**, 731; (*n*) L. Tesi, E. Lucaccini, I. Cimatti, M. Perfetti, M. Mannini, M. Atzori, E. Morra, M. Chiesa, A. Caneschi, L. Sorace and R. Sessoli, Quantum coherence in a processable vanadyl complex: new tools for the search of molecular spin qubits, *Chem. Sci.*, 2016, **7**, 2074.

3 (*a*) F. Neese and D. A. Pantazis, What is not required to make a single molecule magnet, *Faraday Discuss.*, 2011, **148**, 229; (*b*) O. Waldmann, A Criterion for the Anisotropy Barrier in Single-Molecule Magnets, *Inorg. Chem.*, 2007, **46**, 10035.

4 (*a*) R. A. Layfield and M. Murugesu, *Lanthanides and Actinides in Molecular Magnetism*, Wiley-VCH, 2015; (*b*) P. Zhang, Y. Guo and J. Tang, Recent advances in dysprosium-based single molecule magnets: Structural overview and synthetic strategies, *Coord. Chem. Rev.*, 2013, **257**, 1728; (*c*) J. Tang and P. Zhang., *Lanthanide Single Molecule Magnets*, Springer-Verlag, Berlin Heidelberg, 2015; (*d*) K. L. M. Harriman and M. Murugesu, An Organolanthanide Building Block Approach to Single-Molecule Magnets, *Acc. Chem. Res.*, 2016, **49**, 1158; (*e*) J. L. Liu, Y. C. Chen and M. L. Tong, Symmetry strategies for high performance lanthanide-based single-molecule magnets, *Chem. Soc. Rev.*, 2018, **47**, 2431; (*f*) B. M. Day, F. S. Guo and R. A. Layfield, Cyclopentadienyl Ligands in Lanthanide Single-Molecule Magnets: One Ring To Rule Them All?, *Acc. Chem. Res.*, 2018, **51**, 1880; (*g*) M. Feng and M. L. Tong, Single Ion Magnets from 3d to 5f: Developments and Strategies, *Chem. – Eur. J.*, 2018, **24**, 7574; (*h*) A. Dey, P. Kalita and V. Chandrasekhar, Lanthanide(III)-Based Single-Ion Magnets, *ACS Omega*, 2018, **3**, 9462; (*i*) J. Lu, M. Guo and J. Tang, Recent Developments in Lanthanide Single-Molecule Magnets, *Chem. – Asian J.*, 2017, **12**, 2772.

5 (*a*) S. Gómez-Coca, E. Cremades, N. Aliaga-Alcalde and E. Ruiz, Mononuclear Single-Molecule Magnets: Tailoring the Magnetic Anisotropy of First-Row Transition-Metal Complexes, *J. Am. Chem. Soc.*, 2013, **135**, 7010; (*b*) L. Ungur and L. F. Chibotaru, Strategies toward High-Temperature Lanthanide-Based Single-Molecule Magnets, *Inorg. Chem.*, 2016, **55**, 10043; (*c*) N. F. Chilton, C. A. P. Goodwin, D. P. Mills and R. E. P. Winpenny, The first near-linear bis (amide) f-block complex: a blueprint for a high temperature single molecule magnet, *Chem. Commun.*, 2015, **51**, 101.

6 (*a*) J. D. Rinehart and J. R. Long, Exploiting single-ion anisotropy in the design of f-element single-molecule magnets, *Chem. Sci.*, 2011, **2**, 2078; (*b*) I. Oyarzabal, J. Ruiz, J. M. Seco, M. Evangelisti, A. Camón, E. Ruiz, D. Aravena and E. Colacio, Rational Electrostatic Design of Easy-Axis

Magnetic Anisotropy in a ZnII–DyIII–ZnII Single-Molecule Magnet with a High Energy Barrier, *Chem. – Eur. J.*, 2014, **20**, 14262; (*c*) N. F. Chilton, D. Collison, E. J. L. McInnes, R. E. P. Winpenny and A. Soncini, An electrostatic model for the determination of magnetic anisotropy in dysprosium complexes, *Nat. Commun.*, 2013, **4**, 2551.

7 (*a*) T. Pugh, N. F. Chilton and R. A. Layfield, A Low-Symmetry Dysprosium Metallocene Single-Molecule Magnet with a High Anisotropy Barrier, *Angew. Chem., Int. Ed.*, 2016, **55**, 11082; (*b*) C. A. P. Goodwin, F. Ortu, D. Reta, N. F. Chilton and D. P. Mills, Molecular magnetic hysteresis at 60 kelvin in dysprosocenium, *Nature*, 2017, **548**, 439; (*c*) F. S. Guo, B. M. Day, Y. C. Chen, M. L. Tong, A. Mansikkamäki and R. A. Layfield, Magnetic hysteresis up to 80 kelvin in a dysprosium metallocene single-molecule magnet, *Science*, 2018, **362**, 1400.

8 S. Titos-Padilla, J. Ruiz, J. M. Herrera, E. K. Brechin, W. Wersndorfer, F. Lloret and E. Colacio, Dilution-Triggered SMM Behavior under Zero Field in a Luminescent Zn2Dy2 Tetranuclear Complex Incorporating Carbonato-Bridging Ligands Derived from Atmospheric CO2 Fixation, *Inorg. Chem.*, 2013, **52**, 9620.

9 M. J. Giansiracusa, S. Al-Badran, A. K. Kostopoulos, G. F. S. Whitehead, D. Collison, F. Tuna, R. E. P. Winpenny and N. F. Chilton, A large barrier single-molecule magnet without magnetic memory, *Dalton Trans.*, 2019, **48**, 10795.

10 (*a*) A. Lunghi, F. Totti, R. Sessoli and S. Sanvit, The role of anharmonic phonons in under-barrier spin relaxation of single molecule magnets, *Nat. Commun.*, 2017, **8**, 14620; (*b*) J. Escalera-Moreno, J. Baldoví, A. Gaita-Ariño and E. Coronado, Spin states, vibrations and spin relaxation in molecular nanomagnets and spin qubits: a critical perspective, *Chem. Sci.*, 2018, **13**, 3265; (*c*) A. Lunghi, F. Totti, S. Sanvit and R. Sessoli, Intra-molecular origin of the spin-phonon coupling in slow-relaxing molecular magnets, *Chem. Sci.*, 2017, **8**, 6051; (*d*) M. K. Singh, M. Khatua, P. Shukla and G. Rajaraman, A Design Criteria to Achieve a Giant Ising-Type Anisotropy in CoII Encapsulated Metallo-Fullerenes, 2019, DOI: 10.1002/chem.201903618.

11 S. K. Singh, T. Gupta, M. Shanmugam and G. Rajaraman, Unprecedented magnetic relaxation via the fourth excited state in low-coordinate lanthanide single-ion magnets: a theoretical perspective, *Chem. Commun.*, 2014, **50**, 15513; I. Oyarzabal, J. Ruiz, E. Ruiz, D. Aravena, J. M. Seco and E. Colacio, Increasing the effective energy barrier promoted by the change of a counteranion in a Zn–Dy–Zn SMM: slow relaxation via the second excited state, *Chem. Commun.*, 2015, **51**, 12353.

12 (*a*) P. Zhang, L. Zhang, C. Wang, S. Xue, S.-Y. Lin and J. Tang, Equatorially Coordinated Lanthanide Single Ion Magnets, *J. Am. Chem. Soc.*, 2014, **136**, 4484; (*b*) K. L. M. Harriman, J. L. Brosmer, L. Ungur, P. L. Diaconescu and M. Murugesu, Pursuit of Record Breaking Energy Barriers: A Study of Magnetic Axiality in Diamide Ligated DyIII Single-Molecule Magnets, *J. Am. Chem. Soc.*, 2017, **139**, 1420.

13 (*a*) L. Sorace, C. Benelli and D. Gatteschi, Lanthanides in molecular magnetism: old tools in a new field, *Chem. Soc. Rev.*, 2011, **40**, 3092; (*b*) P.-E. Car, M. Perfetti, M. Mannini, A. Favre, A. Caneschi and R. Sessoli, Giant field dependence of the low temperature relaxation of the magnetization in a dysprosium(iii)–DOTA complex, *Chem. Commun.*, 2011, **47**, 3751; (*c*) M. A. AlDamen, J. M. Clemente-Juan, E. Coronado, C. Martí-Gastaldo and A. Gaita-Ariño, Mononuclear Lanthanide Single-Molecule Magnets Based on Polyoxometalates, *J. Am. Chem. Soc.*, 2008, **130**, 8874.

14 (*a*) B. M. Day, F.-S. Guo and R. Layfield, Cyclopentadienyl Ligands in Lanthanide Single-Molecule Magnets: One Ring To Rule Them All?, *Acc. Chem. Res.*, 2018, **51**, 1880; (*b*) A. S.-D. Jiang, B.-W. Wang, H.-L. Sun, Z.-M. Wang and S. Gao, An Organometallic Single-Ion Magnet, *J. Am. Chem. Soc.*, 2011, **133**, 4730; (*c*) J. J. Le Roy, L. Ungur, I. Korobkov, L. F. Chibotaru and M. Murugesu, Coupling Strategies to Enhance Single-Molecule Magnet Properties of Erbium–Cyclooctatetraenyl Complexes, *J. Am. Chem. Soc.*, 2014, **136**, 8003; (*d*) J. J. Le Roy, I. Korobkov, J. E. Kim, J. E. Shelter and M. Murugesu, Structural and magnetic conformation of a cerocene [Ce(COT″)2]– exhibiting a uniconfigurational f^1 ground state and slow-magnetic relaxation, *Dalton Trans.*, 2014, **43**, 2737; (*e*) J. J. Le Roy, S. I. Gorelsky, I. Korobkov and M. Murugesu, Slow Magnetic Relaxation in Uranium(III) and Neodymium(III) Cyclooctatetraenyl Complexes, *Organometallics*, 2015, **34**, 1415; (*f*) L. Münzfeld, C. Schoo, S. Bestgen, E. Moreno-Pineda, R. Köppe, M. Ruben and P. W. Roesky, Synthesis, structures and magnetic properties of [(η9-C9H9)Ln(η8-C8H8)] super sandwich complexes, *Nat. Chem.*, 2019, **10**, 3135, DOI: 10.1038/s41467-019-10976-6.

15 (*a*) Y.-C. Chen, J.-L. Liu, L. Ungur, J. Liu, Q.-W. Li, L.-F. Wang, Z.-P. Ni, L. F. Chibotaru, X.-M. Chen and M.-L. Tong, Symmetry-Supported Magnetic Blocking at 20 K in Pentagonal Bipyramidal Dy(III) Single-Ion Magnets, *J. Am. Chem. Soc.*, 2016, **138**, 2829; (*b*) Y.-S. Ding, N. F. Chilton, R. E. P. Winpenny and Y.-Z. Zheng, On Approaching the Limit of Molecular Magnetic Anisotropy: A Near-Perfect Pentagonal Bipyramidal Dysprosium(III) Single-Molecule Magnet, *Angew. Chem., Int. Ed.*, 2016, **55**, 16071; (*c*) J. Liu, Y.-C. Chen, J.-L. Liu, V. Vieru, L. Ungur, J.-H. Jia, L. F. Chibotaru, Y. Lan, W. Wernsdorfer, S. Gao, X.-M. Chen and M.-L. Tong, A Stable Pentagonal Bipyramidal Dy(III) Single-Ion Magnet with a Record Magnetization Reversal Barrier over 1000 K, *J. Am. Chem. Soc.*, 2016, **138**, 5441; (*d*) S. K. Gupta, T. Rajeshkumar, G. Rajaraman and R. Murugavel, An air-stable Dy(iii) single-ion magnet with high anisotropy barrier and blocking temperature, *Chem. Sci.*, 2016, **7**, 5181; (*e*) J. L. Liu, Y. C. Chen, Y. Z. Zheng, W. Q. Lin, L. Ungur, W. Wernsdorfer, L. F. Chibotaru and M. L. Tong, Switching the anisotropy barrier of a single-ion magnet by symmetry change from quasi-D5 h to quasi-Oh, *Chem. Sci.*, 2013, **4**, 3310; (*f*) Y. C. Chen, J. L. Liu, Y. Lan, Z. Q. Zhong, A. Mansikkamäki, L. Ungur, Q. W. Li, J. H. Jia,

L. F. Chibotaru, J. B. Han, W. Wernsdorfer, X. M. Chen and M. L. Tong, Dynamic Magnetic and Optical Insight into a High Performance Pentagonal Bipyramidal DyIII Single-Ion Magnet, *Chem. – Eur. J.*, 2017, **23**, 5708; (*g*) A. B. Canaj, M. K. Singh, C. Wilson, G. Rajaraman and M. Murrie, Chemical and in silico tuning of the magnetisation reversal barrier in pentagonal bipyramidal Dy(iii) single-ion magnets, *Chem. Commun.*, 2018, **54**, 8273; (*h*) Z. Jiang, L. Sun, Q. Yang, B. Yin, H. Ke, J. Han, Q. Wei, G. Xie and S. Chen, Excess axial electrostatic repulsion as a criterion for pentagonal bipyramidal DyIII single-ion magnets with high U_{eff} and T_B, *J. Mater. Chem. C*, 2018, **6**, 4273; (*i*) Y.-S. Ding, Y.-Q. Zhai, R. E. P. Winpenny and Y.-Z. Zheng, A Simple Magneto-Structural Correlation for Dysprosium(III) Single-Molecule Magnets with Ligands on the Anisotropy Axis, *ChemRxiv*, DOI: 10.26434/chemrxiv.7083038.v1.

16 S. Alvarez, D. Avnir, M. Llunell and M. Pinsky, Continuous symmetry maps and shape classification. The case of six-coordinated metal compounds, *New J. Chem.*, 2002, **26**, 996.

17 (*a*) A. Swain, A. Sarkar and G. Rajaraman, Role of Ab Initio Calculations in the Design and Development of Organometallic Lanthanide-Based Single-Molecule Magnets, *Chem. – Asian J.*, 2019, **2**, DOI: 10.1002/asia.201900828; (*b*) T. Gupta and G. Rajaraman, Modelling spin Hamiltonian parameters of molecular nanomagnets, *Chem. Commun.*, 2016, **52**, 8972.

18 M. J. Giansiracusa, A. K. Kostopoulos, D. Collison, R. E. P. Winpenny and N. F. Chilton, Correlating blocking temperatures with relaxation mechanisms in monometallic single-molecule magnets with high energy barriers (Ueff > 600 K), *Chem. Commun.*, 2019, **55**, 7025.

19 G. M. A. Sheldrick, Short history of SHELX, *Acta Crystallogr.*, 2008, **64**, 112–122.

20 O. V. Dolomanov, L. J. Bourhis, R. J. Gildea, J. A. K. Howard and H. Puschmann, OLEX2: a complete structure solution, refinement and analysis program, *J. Appl. Crystallogr.*, 2009, **42**, 339–341.

21 F. Aquilante, J. Autschbach, R. K. Carlson, L. F. Chibotaru, M. G. Delcey, L. De Vico, I. Fdez Galván, N. Ferré, L. M. Frutos, L. Gagliardi, M. Garavelli, A. Giussani, C. E. Hoyer, G. Li Manni, H. Lischka, D. Ma, P. Å. Malmqvist, T. Müller, A. Nenov, M. Olivucci, T. B. Pedersen, D. Peng, F. Plasser, B. Pritchard, M. Reiher, I. Rivalta, I. Schapiro, J. Segarra-Martí, M. Stenrup, D. G. Truhlar, L. Ungur, A. Valentini, S. Vancoillie, V. Veryazov, V. P. Vysotskiy, O. Weingart, F. Zapata and R. Lindh, Molcas 8: New capabilities for multiconfigurational quantum chemical calculations across the periodic table, *J. Comput. Chem.*, 2016, **37**, 506.

22 H. Nojiri, K.-Y. Choi and N. Kitamura, Manipulation of the quantum tunneling of nanomagnets by using time-dependent high magnetic fields, *J. Magn. Magn. Mater.*, 2007, **310**, 1468.

23 L. F. Chibotaru and L. Ungur, Ab initio calculation of anisotropic magnetic properties of complexes. I. Unique definition of pseudospin Hamiltonians and their derivation, *J. Chem. Phys.*, 2012, **137**, 064112.

24 (*a*) B. O. Roos, V. Veryazov and P. O. Widmark, Relativistic atomic natural orbital type basis sets for the alkaline and alkaline-earth atoms applied to the ground-state potentials for the corresponding dimers, *Theor. Chim. Acta*, 2004, **111**, 345; (*b*) B. O. Roos, R. Lindh, P. A. Malmqvist, V. Veryazov and P. O. Widmark, Main Group Atoms and Dimers Studied with a New Relativistic ANO Basis Set, *J. Phys. Chem. A*, 2004, **108**, 2851; (*c*) B. O. Roos, R. Lindhn, P. A. Malmqvist, V. Veryazov and P. O. Widmark, New Relativistic ANO Basis Sets for Transition Metal Atoms, *J. Phys. Chem. A*, 2005, **109**, 6575; (*d*) B. O. Roos, R. Lindh, P. A. Malmqvist, V. Veryazov and P. O. Widmark, New relativistic ANO basis sets for actinide atoms, *Chem. Phys. Lett.*, 2005, **409**, 295.

25 H. Koch, A. Sánchez de Merás and J. Pedersen, Reduced scaling in electronic structure calculations using Cholesky decompositions, *J. Chem. Phys.*, 2003, **118**, 9481.

26 B. O. Roos, P. R. Taylor and P. E. M. Siegbahn, A complete active space SCF method (CASSCF) using a density matrix formulated super-CI approach, *Chem. Phys.*, 1980, **48**, 157.

27 B. O. Roos and P. Malmqvist, Relativistic quantum chemistry: the multiconfigurational approach, *Phys. Chem. Chem. Phys.*, 2004, **6**, 2919.

28 L. Gagliardi, R. Lindh and G. Karlstrom, Local properties of quantum chemical systems: The LoProp approach, *J. Chem. Phys.*, 2004, **121**, 4494.